IEEE Access
Multidisciplinary | Rapid Review | Open Access Journal

IEEE POWER & ENERGY SOCIETY SECTION

Received 10 December 2024, accepted 3 January 2025, date of publication 10 January 2025, date of current version 15 January 2025.

Digital Object Identifier 10.1109/ACCESS.2025.3528296

RESEARCH ARTICLE

Signal Processing-Free Intelligent Model for Power Quality Disturbances Identification

MOHAMMED F. AL-MASHDALI[1], ASIF ISLAM[1,2,3], (Member, IEEE), ABDULBASIT HASSAN[4,5], (Student Member, IEEE), MD SHAFIULLAH[2,4], (Senior Member, IEEE), MUJAHED AL-DHAIFALLAH[2,4], (Member, IEEE), AND KHALID AL FUWAIL[4], (Member, IEEE)

[1]Electrical Engineering Department, King Fahd University of Petroleum and Minerals, Dhahran 31261, Saudi Arabia
[2]Interdisciplinary Research Center for Sustainable Energy Systems, King Fahd University of Petroleum and Minerals, Dhahran 31261, Saudi Arabia
[3]High Voltage Laboratory, King Fahd University of Petroleum and Minerals, Dhahran 31261, Saudi Arabia
[4]Control and Instrumentation Engineering Department, King Fahd University of Petroleum and Minerals, Dhahran 31261, Saudi Arabia
[5]Air Force Institute of Technology, Kaduna, Nigeria

Corresponding author: Md Shafiullah (shafiullah@kfupm.edu.sa)

This work was supported by the Interdisciplinary Research Center for Sustainable Energy Systems (IRC-SES), King Fahd University of Petroleum and Minerals (KFUPM), under Grant INSE2409. The work of Md Shafiullah and Mujahed Al-Dhaifallah was supported by the King Abdullah City for Atomic and Renewable Energy (K.A.CARE).

ABSTRACT Integrating different types of renewable energy sources in the power system substantially challenges the power quality (PQ), directly affecting the system's stability and service life span. The rise of power quality disturbances (PQD) generates irregularities in voltage and current waveforms, harming smart grid networks and linked devices. Traditional methods for PQD classification use complicated feature extraction techniques, which can be computationally expensive and lack scalability. This research proposes applying basic convolutional neural network (CNN) models for automated PQD detection and categorization as a prospective solution to these issues. By directly examining PQD images generated from signal data, these models reduce the requirement for human-crafted features. The study analyzes alternative CNN setups, training datasets, and disturbance types to measure model performance. The results demonstrate that these simple CNN models maintain stable accuracy values in normal and noisy environments, even with increasing classes and noise, the models managed to maintain a high-performance level with up to 99.39% accuracy for 17 classes when the Adam optimizer was used instead of RMSprop. The models could deal with noise-related disturbances, still achieving accuracy as high as 96.42% when trained by just 50% of the dataset under 30dB SNR (Signal to Noise Ratio) conditions. Moreover, comparing the two frequencies on 50Hz and 60Hz performance does not show the equivalent models' robustness over different operating levels. This study highlights the potential of CNNs in boosting power quality disturbance categorization and presents paths for further inquiry in model refining and optimization. The study focuses on CNN-based models applied in power quality disturbance detection and classification research.

INDEX TERMS Convolutional neural networks (CNN), power quality (PQ), renewable energy, machine learning.

I. INTRODUCTION

In modern times, the power system is confronted with a considerable problem in preserving power quality owing to its integration with varied renewable energy sources. Harmonic distortions from this integration, like solar systems, can lead to voltage swings and increased losses, necessitating effective mitigation strategies to enhance power quality [1]. This integration has a direct influence on the stability of the power system, making PQ management a significant problem [2].

The associate editor coordinating the review of this manuscript and approving it for publication was Emilio Barocio.

© 2025 The Authors. This work is licensed under a Creative Commons Attribution 4.0 License.
For more information, see https://creativecommons.org/licenses/by/4.0/

PQ refers to a wide range of electromagnetic events that cause deviations from the expected waveforms of voltage and current. These deviations are power quality disturbances [3]. These disturbances might impact smart grid networks and the electrical equipment they link in many ways, from little glitches to significant outages. This may make the smart grid networks less safe and more costly to operate, and it may also impair the lifetime and performance of the electrical equipment [2], [3]. Therefore, promptly recognizing and precisely categorizing these disturbances using an intelligent and automated approach is vital to sustaining a stable power supply.

While the protection relays provide the decision-making part of switchgear, therefore for protection tasks, the fault detection algorithms are installed in the relay. According to the ANSI/IEEE C37.60 [4], Figure 1 represents the 'unit operation' illustration of protection switchgear. IEC 62271-111 [5], and IEC 62271-200 standard [6]. According to the diagram, all other events are electromechanical except the release delay, which also does not depend on the protection algorithm. Release delay is the operating time of the protection algorithm and is defined as the time from when the fault occurs to when the protection operation is triggered. This time varies depending on the fault detection algorithm and protection settings configured. Therefore, this paper focuses on the 'release delay' part of the unit operation of a switchgear.

This research aims to investigate the effectiveness of simple CNN models in accurately identifying and classifying PQDs without the need for signal processing techniques.

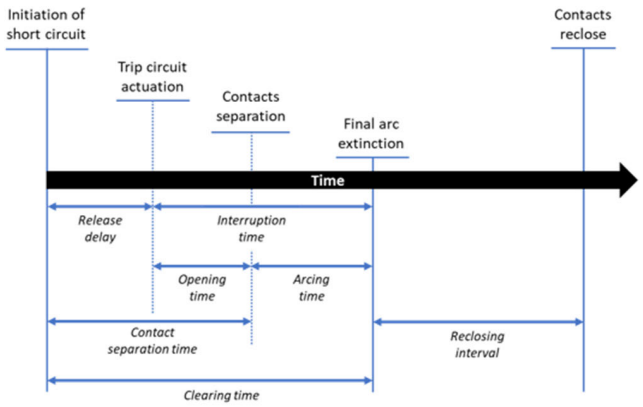

FIGURE 1. Unit operation of load/fault-current interruption and contacts reclosing [4].

The procedure we have adopted is to first review in Section II the existing methodologies to detect PQD and the application of CNN for a similar purpose and compare the other works done using different neural networks. Then, in Section III of the paper, we discussed an overview of the process used to generate PQD images and the CNN approach. The results from different CNN models with varied parameters are reviewed and compared in Section IV. At the same time, the implication of the proposed technique in conventional protection relays is focused on in Section V. Finally, the concluding section summarizes the outcome of this paper with directions to future research opportunities.

This paper contributes to the field of Power Quality Disturbance identification and classification in several ways:

- It introduces the idea of using a simple Convolutional Neural Network (CNN) model that skips traditional signal processing methods, thus decreasing the computational cost and domain knowledge needed for feature extraction.
- The study evaluates and compares various convolutional neural network setups, training datasets, and disturbance types to assess the model's performance under diverse conditions, including high noise levels. This investigation provides a perception of the proposed model's robustness.
- The proposed CNN models demonstrate scalability and computational efficiency, by achieving a high accuracy in distinguishing PQDs across multiple classes with minimal pre-processing tasks.
- This study highlights the application of proposed the model for real-time power quality disturbance detection in conventional protection relays for advanced grid systems monitoring.

Together, these contributions will harness effective power quality monitoring solutions for smart grid systems.

II. BACKGROUND OF THE STUDY

Intelligent models hold significant potential for practical applications in the identification of power quality disturbances for smart grid systems and renewable energy integration [7]. According to past studies on PQDs, two main steps are often involved in determining PQDs: feature extraction and classification. Traditional feature extractions mostly include signal processing techniques such as Hilbert-Huang transform (HHT), short-time Fourier transform (STFT), Wigner-Ville distribution (WVD), variational mode decomposition (VMD) S-transform (ST), Fast Fourier Transformation (FFT), Fourier transform (FT), and wavelet transform (WT), [8], [9], [10], [11], [12], [13], [14], [15], [16], [17], [18], [19]. However, these approaches include some downsides, such as high computational costs, dependency on human feature extraction and selection, and limits in scalability and reliability [20]. For these reasons, simple deep-learning approaches are suggested in this study for categorizing PQDs. The goal is to bypass the feature extraction step and make feature extraction automatic with the classification process. In the literature, CNN has become more widespread for feature extraction and classification as a deep learning algorithm and has proven its efficiency in image classification more than the other state-of-the-art techniques. While Recurrent Neural Networks (RNNs) and Long Short-Term Memory networks (LSTMs) are more suited for sequence-based data and excel in time-series prediction, they are not designed to capture spatial patterns from image data [21]. The benefit of the CNN algorithm is its capacity

to automatically discover optimal features from raw input data by exploiting many layers of abstraction and representation [22]. In earlier research, CNN approaches were applied to the identification of PQDs. These approaches include using CNN models to estimate voltage sags in power systems with limited monitoring [23].

These models significantly enhance the reliability and efficiency of power systems by accurately detecting and classifying disturbances, which are essential for maintaining power quality and renewable energy integration. Therefore, the application of advanced machine learning techniques can provide precise monitoring of power quality for improved energy management and enhanced cost efficiency. In a smooth power quality monitoring, Ref. [24] proposed an intelligent model using deep neural networks together with time-frequency feature fusion. The model demonstrated high accuracy in identifying power quality disturbances, even with varying hyperparameters. Similarly, Ref. [25] highlights the use of CNNs and Gated Recurrent Units (GRUs), for the accurate identification of both single and complex disturbances. This approach significantly improves system diagnostics and reliability. For efficient data processing and real-time monitoring, A proposed model by Ref. [26] reduces computational complexity and processing time, by combining data compression techniques with CNN classification to enable effective detection of power quality disturbance data. Intelligent models enable the continuous integration of renewable energy sources by effectively managing random and nonlinear loads, this contributes to robust and reliable operation in modern energy infrastructures [27]. Also, intelligent models are capable of managing the temporal variability introduced by renewable energy sources, thereby ensuring stable and efficient operation of the power grid [25].

Furthermore, CNN has been combined with other signal-processing techniques [7], integrated with long short-term memory (LSTM) networks [28], employed in conjunction with phase space reconstruction (PSR) [29], and utilized deep belief networks (DBNs) [30]. Additionally, the combination of 1D power signals and 2D signal images has been explored [31], as has the integration of CNN with GRU models [32]. Even though these methods have shown positive results, their systems are still complex and have problems handling more PQD types. This research discusses the background of basic and uncomplicated models based on CNN for detecting and classifying PQD. The primary purpose is to study the efficiency of these models in providing excellent results and reaching high levels of accuracy. Different quantities of data, training sets, and several types are explored to test the performance of the suggested models in handling PQD identification and classification tasks.

III. METHODOLOGY

This section will describe the equations applied, the values required to produce the PQD database provided as images, and the number of disturbance types generated using Python. Furthermore, the suggested technique will be implemented utilizing a simple CNN framework with different parameters.

A. PQDS MODELING AND DATA PREPARATION

Table 1 contains information on 19 different types of PQD signals, including their characteristic equations and typical parameters according to the international standards in [33], [34], and [35]. These signals were created as images using Python through the Jupyter Notebook environment [36], and Figure 2 presents a simple example for each class. The signals were generated with particular constants: The generated signal images were recorded for 20 seconds with these values: normalized amplitudes to 1 p.u., 60 Hz is the fundamental frequency, and the sampling frequency is 10 kHz. Two signals were also created: one with no noise and the other with a 30 dB signal-to-noise ratio.

B. CNN'S PROPOSED FRAMEWORK

CNN, which stands for Convolutional Neural Network, is a widely used deep learning method in computer vision, enabling tasks such as image recognition, object detection, and image categorization [22]. A typical CNN design comprises numerous layers, including convolutional, pooling, and fully connected layers. The output of each layer is represented by a collection of activation values [37].

The mathematical depiction of a CNN architecture is as follows:

$$Y = f(Xw + b) \tag{1}$$

The activation function is defined by f, w represent the weight matrix Y and X are the output and input layer respectively, b is the bias term.

To improve pattern recognition, activation functions are applied to the outputs of neural network layers. A Conv2D layer is employed in this study to conduct a 2D convolution operation on the input tensor. Convolution is performed by sliding a tiny filter window, referred to as a kernel, over the input tensor and computing the dot product between the kernel and the corresponding input patch. The Conv2D operation has the following mathematical expression:

$$Y_1 = fr(conv2d(X, w) + b) \tag{2}$$

Y_1 represent the output of the Conv2D layer, and $conv2d()$ is the convolution operation.

The expression for the Rectified Linear Unit (ReLU) function can be written as:

$$fr(x) = max(0, x) \tag{3}$$

A MaxPooling2D layer takes the maximum value within a short window to down sample the input tensor. The MaxPooling2D operation has the following mathematical expression:

$$Y_3 = f(Xn) = argmax(Xn) \tag{4}$$

Y_3 is the output of the MaxPooling2D layer, and Xn is the vector that holds the pooled data.

TABLE 1. Mathematical models of PQDs.

	Label	Equation	Parameter
Pure signal	C0	$[1 \pm \alpha(\mathrm{u}(\mathrm{t}-t_1)-\mathrm{u}(\mathrm{t}-\mathrm{t}_2))]\sin(\omega t)$	$\alpha < 0.04, \mathrm{T} \le (\mathrm{t}_2-\mathrm{t}_1) \le 9\ \mathrm{T}$
Swell	C1	$[1+\alpha(u(t-\mathrm{t}_1)-u(t-\mathrm{t}_2))]\sin(\omega t)$	$0.1 \le \alpha \le \underline{08}\ \mathrm{T}\ \mathrm{T} \le (\mathrm{t}_2-\mathrm{t}_1) \le 9\ \mathrm{T}$
Sag	C2	$[1-\alpha(u(t-\mathrm{t}_1)-u(t-\mathrm{t}_2))]\sin(\omega t)$	$0.1 \le \alpha < 0.9, \mathrm{T} \le (\mathrm{t}_2-\mathrm{t}_1) \le 9\ \mathrm{T}$
Interruption	C3	$[1-\alpha(u(t-\mathrm{t}_1)-\mathrm{u}(\mathrm{t}-\mathrm{t}_2)\ )]\ \sin(\omega t)$	$0.9 \le \alpha \le 1, \mathrm{T} \le (\mathrm{t}_2-\mathrm{t}_1) \le 9\ \mathrm{T}$
Harmonics	C4	$\alpha\sin(\omega t)+3\alpha\sin(3\omega t)+5\alpha\sin(5\omega t)+7\alpha\sin(7\omega t)$	$0.05 \le \alpha 3, \alpha 5, \alpha 7 \le 0.15, \alpha 1 = 1$
Flicker	C5	$[1+\alpha f\sin(\beta\omega t)]\sin(\omega t)$	$0.1 \le \alpha f \le 0.2, 0.05 \le \beta \le 0.5$
Impulsive transient	C6	$[1-\alpha(\mathrm{u}(\mathrm{t}-\mathrm{t}_1)-\mathrm{u}(\mathrm{t}-\mathrm{t}_2)\ )]\ \sin(\omega t)$	$1 \le \alpha \le 4.14, \mathrm{T}/30 \le (\mathrm{t}_2-\mathrm{t}_1) \le \mathrm{T}$
Oscillatory transient	C7	$\sin(\omega t)+\alpha-(\mathrm{t}-\mathrm{t}_1)/\tau\sin(\omega_n(t-\mathrm{t}_1))(\mathrm{u}(\mathrm{t}_2)-\mathrm{u}(\mathrm{t}_1))$	$0.1 < \alpha \le 0.8, 0.5\ \mathrm{T} \le (\mathrm{t}_2-\mathrm{t}_1) \le 3\ \mathrm{T}$ $, 8 \le \tau \le 40\ \mathrm{ms}, 30 \le 2\pi\omega_n \le 90\mathrm{kHz}$
Notch	C8	$\sin(\omega t)-\mathrm{sign}(\sin(\omega t)) \times \sum 9\mathrm{n}=0\mathrm{k}[\mathrm{u}(\mathrm{t}-(\mathrm{t}_1-0.02\mathrm{n}))$ $-\mathrm{u}(\mathrm{t}-(\mathrm{t}_2-0.02\mathrm{n}))]$	$0.1 \le \mathrm{K} \le 0.4, 0.01\ \mathrm{T} \le \mathrm{t}_2-\mathrm{t}_1$ $\le 0.05\ \mathrm{T}$
Spike	C9	$\sin(\omega t)+\mathrm{sign}(\sin(\omega t)) \times \sum 9\mathrm{n}=0\mathrm{k}[\mathrm{u}(\mathrm{t}-(\mathrm{t}_1-0.02\mathrm{n}))$ $-\mathrm{u}(\mathrm{t}-(\mathrm{t}_2-0.02\mathrm{n}))]$	
Harmonics+Swell	C10	$[1+\alpha(\mathrm{u}(\mathrm{t}-\mathrm{t}_1)-\mathrm{u}(\mathrm{t}-\mathrm{t}_2))] \times [\alpha 1\sin(\omega t)+\cdots+$ $7\alpha\sin(7\omega t)]$	combine
Harmonics+Sag	C11	$[1-\alpha(\mathrm{u}(\mathrm{t}-\mathrm{t}_1)-\mathrm{u}(\mathrm{t}-\mathrm{t}_2))] \times [\alpha 1\sin(\omega t)+\cdots+$ $7\alpha\sin(7\omega t)]$	
Harmonics+Interruption	C12	$[1-\alpha(\mathrm{u}(\mathrm{t}-\mathrm{t}_1)-\mathrm{u}(\mathrm{t}-\mathrm{t}_2))] \times [\alpha 1\sin(\omega t)+\cdots+$ $7\alpha\sin(7\omega t)]$	
Harmonics+Flicker	C13	$[1+\alpha f\sin(\beta\omega t)] \times [\alpha 1\sin(\omega t)+\cdots+\alpha 7\sin(7\omega t)]$	
Oscillatory transient+Harmonics	C14	$[\sin(\omega t)+\alpha-((\mathrm{t}-\mathrm{t}_1)/\mathrm{t})\sin(\omega_n(\mathrm{t}-\mathrm{t}_1))(\mathrm{u}(\mathrm{t}_2)-\mathrm{u}(\mathrm{t}1))] \times$ $[\alpha\sin(\varphi\mathrm{t})+\cdots+7\alpha\sin(7\omega t)]$	
Flicker+Swell	C15	$[1+\alpha f\sin(\beta\omega t)][1+\alpha(u(t-\mathrm{t}_1)-u(t-\mathrm{t}_2))]\sin(\omega t)$	
Flicker+Sag	C16	$[1+\alpha f\sin(\beta\omega t)][1-\alpha(u(t-\mathrm{t}_1)-u(t-\mathrm{t}_2))]\sin(\omega t)$	
Oscillatory transient+Swell	C17	$[\sin(\omega t)+\alpha-((\mathrm{t}-\mathrm{t}_1)/\tau)\sin(\omega_n(\mathrm{t}-\mathrm{t}_1))(\mathrm{u}(\mathrm{t}_2)-\mathrm{u}(\mathrm{t}_1))] \times$ $[1+\alpha(\mathrm{u}(\mathrm{t}-\mathrm{t}_1)-\mathrm{u}(\mathrm{t}-\mathrm{t}_2))]$	
Oscillatory transient+Sag	C18	$[\sin(\omega t)+\alpha-((\mathrm{t}-\mathrm{t}_1)/\tau)\sin(\omega_n(\mathrm{t}-\mathrm{t}_1))(\mathrm{u}(\mathrm{t}_2)-\mathrm{u}(\mathrm{t}_1))] \times$ $[1-\alpha(\mathrm{u}(\mathrm{t}-\mathrm{t}_1)-\mathrm{u}(\mathrm{t}-\mathrm{t}_2))]$	

The Flatten layer converts the input tensor to a 1D vector. The mathematical expression for the Flatten operation is as follows:

$$Y_4 = X.reshape(-1) \tag{5}$$

where, reshape () is an automatic inference to flatten.

Finally, the dense layer connects every neuron from the previous layer with every neuron from the current layer to make a critical decision. The mathematical expression for the Dense operation is as follows:

$$Y_5 = fr(Xw + b) \tag{6}$$

$Y_5$is the output of the dense layer after the other layers have been applied.

Figure 3 shows the suggested method's framework and summarizes its structure. Table 2 shows the model's varied parameters. The CNN model receives the PQD images directly after the image data for various PQD signal types is created. The main goal of this stage is to correctly identify the PQD images based on the various disturbance types by extracting distinctive features from the images and classifying them accurately.

The proposed method in this work is separated into three parts, each corresponding to a different number of input classes for the CNN model, as shown in Table 3. In general,

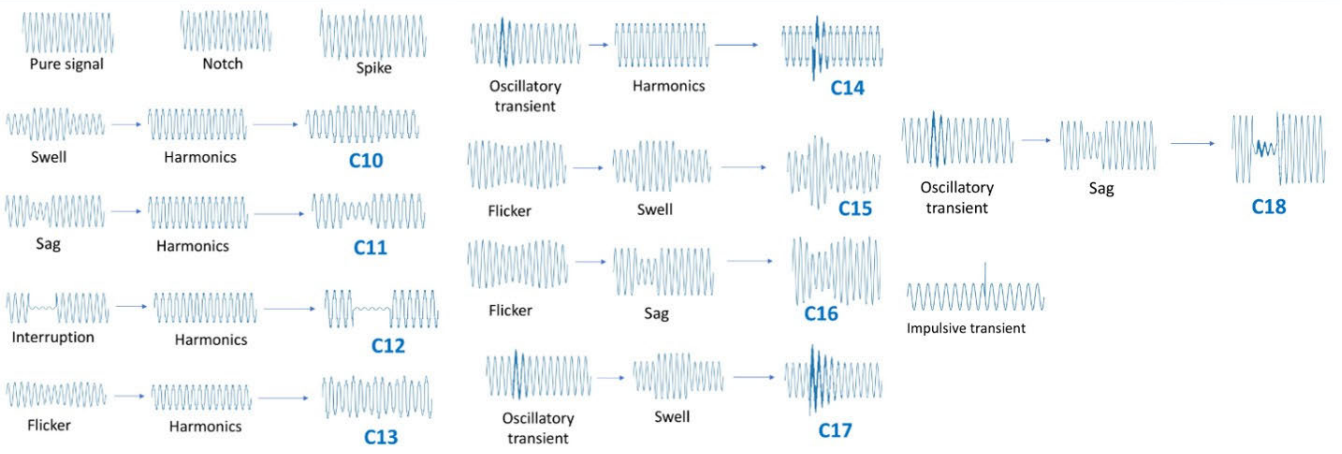

FIGURE 2. Nineteen test classes as elaborated in Table 1.

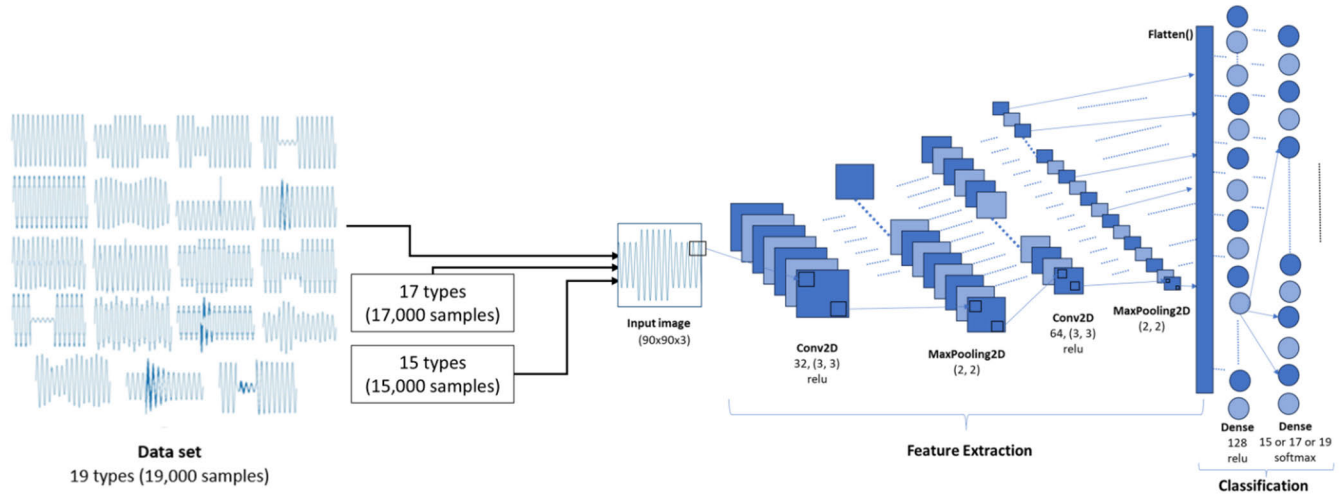

FIGURE 3. Proposed methodology.

the CNN model has a consistent structure. It begins with an input image of size 90 × 90, which is then passed through convolutional layers with 32 and 64 filters of size 3 × 3, respectively. The ReLU activation function is utilized to introduce non-linearity. Subsequently, max-pooling layers with a pool size of 2 × 2 are applied after each convolutional layer to down-sample the spatial dimensions. The output generated by the last convolutional layer is flattened into a 1D vector. Two fully connected (dense) layers are added to further process the characteristics collected from the CNN. The first dense layer comprises 128 units and utilizes the ReLU activation function. The last dense layer has a variable number of units, either 15, 17, or 19, depending on the specific stage of the suggested approach. The softmax activation function is applied in the final dense layer to classify the input into the corresponding perturbation classes.

The CNN Model for training, classification, and evaluation models was run on a device with an Intel (R) Core (TM) i7-8565U CPU at 1.80 GHz and 1.99 GHz, 8.00 GB of RAM (7.82 GB usable), and an NVIDIA GeForce MX230 graphic card. When dealing with 15 classes in the first part, the data is split into three groups: 80% for training, 10% for testing, and 10% for validation. Another strategy, where the data is divided into 70% for training, 15% for testing, and 30% for validation, is also considered. As shown in Table 3, these divisions are applied to various data sizes. The data is split into the same three sets in the second and third situations, which involve 17 and 18 classes, respectively: 80% for training, 10% for testing, and 10% for validation, and they are applied to various data sizes as in the first scenario, as shown in Table 3.

IV. RESULTS AND DISCUSSIONS

A dataset of images was created for 15 different classes of PQD (this is referred to as Part A). One thousand signal samples were included in each category. The dataset was later expanded to include 17 classes by adding two more types (Part B). Finally, two more classes were added, giving the dataset (Part C) 19 classes. By keeping the same amount of

TABLE 2. Parameters of CNN model for PQDs classification.

Parameter	Value
Data per class	100%,50%,10%* (1000)
Train set	80%,70%
Test set	10%,15%
Validation set	10%,15%
Input Image Size	90 x 90
Batch Size	32
Convolutional Layers	1,2
Convolutional Layer Sizes	32, 64 (Conv2D)
Convolutional Activations	relu, relu
Pooling Layers	1,2 (MaxPooling Layers)
Pooling Layer Sizes	2, 2
Dense Layers	2
Dense Layer Sizes	(128, 19), (128, 17), (128,14)
Dense Layer Activations	relu, softmax
Output Size	15,17,19 (classes)
Loss Function	Categorical Crossentropy
Optimizer	Adam, RMSprop
Training Epochs	10

TABLE 3. Methods' parameters.

	15 classes	17 & 18 classes
% of data	100%,50%,10%* (1000)	100%,50%,10%* (1000)
Train set (%)	80,70	80
Test & Val set (%)	(10,10),(15,15)	10,10
Convolutional Layers	1,2	2
Optimizer	Adam	Adam, RMSprop

data for each class, the aim was to compare those subgroups. To do this, three different scenarios were considered using 100%, 50%, and 10% of the entire data for each class.

A. PART A: 15 CLASSES

Commencing with Table 4, models were trained and assessed using an 80% training and 10% testing and validation split on a dataset with 15 classes. The objective was to evaluate robustness and accuracy in noisy situations. Data proportions, convolutional layers, test accuracy, and accuracy at 30 dB SNR are all listed in Table 4, along with other model information. As a result, Model 1 showed resistance to noise and had a high accuracy of 99.40%. The accuracy of Model 3 was somewhat greater at 99.60%, but it showed a little drop in the presence of noise. Using only 50% of the input and two convolutional layers, Model 4 outperformed the competition with a remarkable accuracy of 99.87%. Due to the small amount of training data, Models 5 and 6 had less accuracy and were susceptible to noise. The comparison highlights the trade-off between accuracy and robustness by emphasizing the relationship between dataset size, model complexity, and noise resilience. Referring to Table 5, the only change between Table 4 and Table 5 is the data division into 70% for training

TABLE 4. 15 classes (80% training, 10% testing, 10%val).

S	% of Data	Convolution Layers	Test Accuracy (%)	with 30 dB SNR (%)
1	100	1	99.40	99.40
2	100	2	98.80	99.40
3	50	1	99.60	99.47
4	50	2	99.87	99.60
5	10	1	97.33	97.33
6	10	2	96.67	95.33

TABLE 5. 15 classes (70% training, 15% testing, 15% val).

S	% of Data	Convolution Layers	Test Accuracy (%)	with 30dB SNR (%)
1	100	1	98.49	99.33
2	100	2	99.60	99.24
3	50	1	99.20	99.20
4	50	2	99.38	99.64
5	10	1	97.33	98.22
6	10	2	94.22	95.11

and 10% each for testing and validation. Because of Table 5, Model 2 employed the entire dataset for training and testing, generating an excellent accuracy of 99.60% on the test set. Two convolutional layers were added, which enhanced its performance. Using 50% of the data and two convolutional layers, Model 4 likewise demonstrated astounding accuracy, scoring 99.38% on the test set and 99.64% under the 30 dB SNR condition.

Table 4 and Table 5 are compared in Figure 4 to show that the test accuracy is marginally higher when the model is trained with 80% rather than 70% of the data. This finding implies that a larger training dataset typically increases performance on unobserved data. The justification for this is that the model may learn and capture a more thorough understanding of the underlying patterns and variances in the data with more data. As a result, it improves at making precise predictions in unanticipated and unfamiliar situations.

B. PART B: 17 CLASSES

A dataset made up of 17 classes was used in the study's second section. While Table 6 used the Adam optimizer, Table 6 used the RMSprop optimizer. The dataset was thoughtfully divided into 10% for testing and 10% for validation, with 80% used for training. The emphasis was on comparing various model setups, focusing on test precision and performance in a 30 dB SNR setting. The Adam optimizer findings in Table 6 were excellent. Model 1 had a commendable test accuracy of 99.29% after being trained on the entire dataset, and this figure increased to 99.59% under the 30 dB SNR condition.

TABLE 6. 17 classes, Adam optimizer.

M	% of Data	Test Accuracy (%)	with 30 dB SNR (%)
1	100	99.29	99.59
2	50	98.35	97.53
3	10	95.29	92.63

TABLE 7. 17 classes, RMSprop optimizer.

M	% of Data	Test Accuracy (%)	with 30 dB SNR (%)
1	100	99.35	99.24
2	50	98.47	99.18
3	10	91.76	98.24

TABLE 8. 19 classes, Adam optimizer.

M	% of Data	Test Accuracy (%)	with 30 dB SNR (%)
1	100	98.16	99.05
2	50	97.79	97.79
3	10	96.32	93.53

TABLE 9. 19 classes, RMSprop optimizer.

M	% of Data	Test Accuracy (%)	with 30 dB SNR (%)
1	100	98.84	98.79
2	50	98.84	96.42
3	10	96.32	93.16

With a test accuracy of 98.35%, Model 2 demonstrated strong performance.

However, when noise was present, the accuracy only marginally fell to 97.53%. Model 3 showed a lower test accuracy of 95.29% and experienced a significant decline to 92.63% in the 30 dB SNR setting. Model 3 was trained on only 10% of the data. Referring to Table 7 (RMSprop optimizer), Model 1 maintained a high accuracy of 99.24% in the 30 dB SNR condition while achieving a noteworthy test accuracy of 99.35% when trained on the complete dataset. Model 2, trained with half of the data, displayed a remarkable accuracy of 99.18% in noisy settings and a respectable test accuracy of 98.47%. Model 3, on the other hand, showed a noticeably lower test accuracy of 91.76% despite having only been trained on 10% of the data. Notably, in the 30 dB SNR setting, its accuracy increased dramatically to 98.24%, demonstrating increased noise resistance. As seen in Figure 5, which contrasts the Adam and RMSprop optimizers, the Adam optimizer consistently produced somewhat greater test accuracy across various models, training data proportions, and normal conditions.

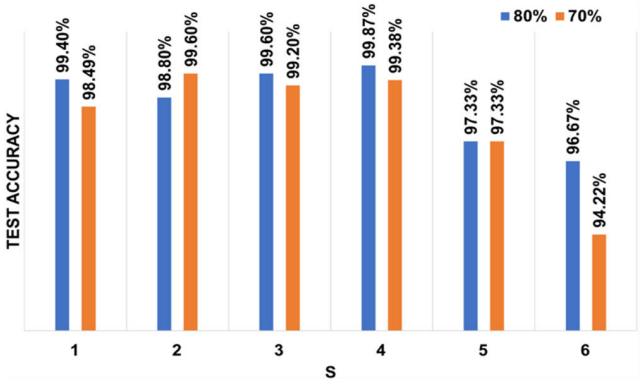

FIGURE 4. Test accuracy comparison: 80% training set vs. 70% training set.

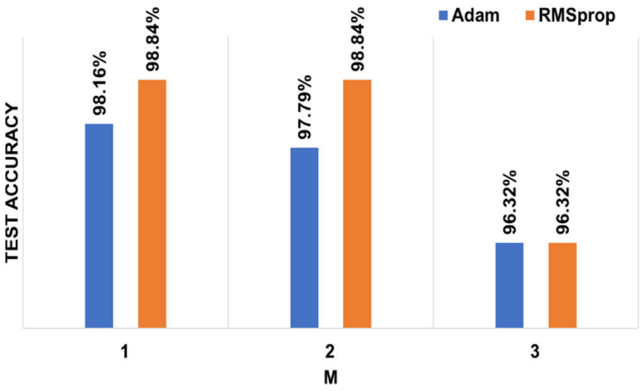

FIGURE 5. Test accuracy comparison: Adam vs. RMSprop.

C. PART C: 19 CLASSES

The last part used a dataset made up of 19 classes. While Table 8 used the Adam optimizer, Table 9 used the RMSprop optimizer. The dataset was thoughtfully split into three sections: training (80%), testing (10%), and validation (10%). Comparing various model configurations was the primary objective, focusing on test accuracy and performance in a 30 dB SNR setting. In Table 8, Model 1 had a noteworthy test accuracy of 98.16% and utilized the entire dataset for training and testing. Impressively, the model displayed a robust accuracy of 99.05% even in the challenging 30 dB SNR condition. With a test accuracy of 97.79% and consistent performance even in the presence of noise, Model 2, trained on 50% of the data, showed passable performance. Table 9 shows that Model 1 had a commendable test accuracy of 98.84% while using the entire dataset.

Surprisingly, the model demonstrated resilient performance, retaining an accuracy of 98.79% even under the demanding 30 dB SNR settings. Similar to Model 1, Model 2 showed a robust test accuracy of 98.84% while maintaining an accuracy of 96.42% in the presence of noise. Model 2 was trained on 50% of the data. Model 3, on the other hand, displayed an excellent test accuracy of 96.32% despite having only been trained on 10% of the data. The small training dataset is to blame for the minor drop in accuracy. Model

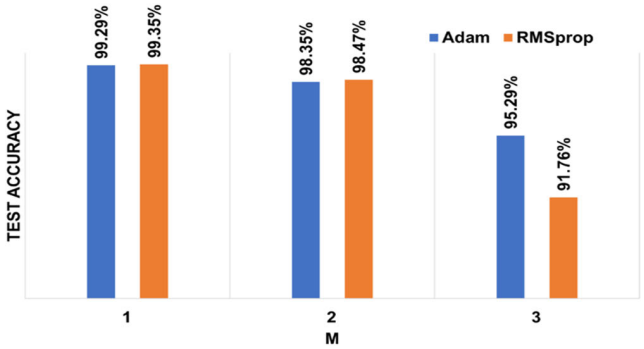

FIGURE 6. Test accuracy comparison: Adam vs. RMSprop.

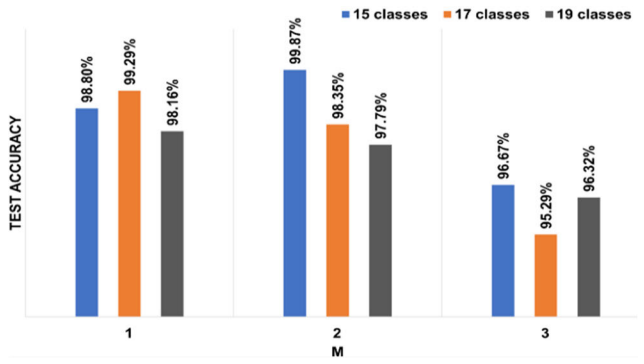

FIGURE 7. Test accuracy comparison: 15 vs. 17 vs. 19 classes.

3's accuracy decreased to 93.16% when tested in a 30 dB SNR setting, demonstrating some noise vulnerability due to the sparse data. Figure 6, which contrasts the Adam and RMSprop optimizers, shows that the RMSprop optimizer consistently produced greater test accuracy across various models, training data proportions, and normal conditions.

D. COMPARISON AND ANALYSIS

Examining test accuracy in Table 10 provides insights into the relationship between the number of classes and model performance. A clear trend emerges by comparing models trained with varying fractions of data and evaluated under standard settings and a 30 dB SNR. Figure 7 and Table 10 demonstrate that when the number of classes grows, there is often a slight decrease in test accuracy across all data proportions. This tendency is maintained when comparing sections I, II, and III, which have 15, 17, and 19 classes. The complexity supplied by a growing number of classes makes it more complicated for models to differentiate and categorize a broader range of items. Figures 8, 9, and 10 show the performance of the models for the three parts (A, B, C), followed by Figures 11, 12, and 13 showing their confusion matrices with test sets.

Interestingly, this tendency continues in the 30 dB SNR case. The introduction of noise further increases the accuracy drop associated with more classes. However, even with this loss, the models still display substantial accuracy,

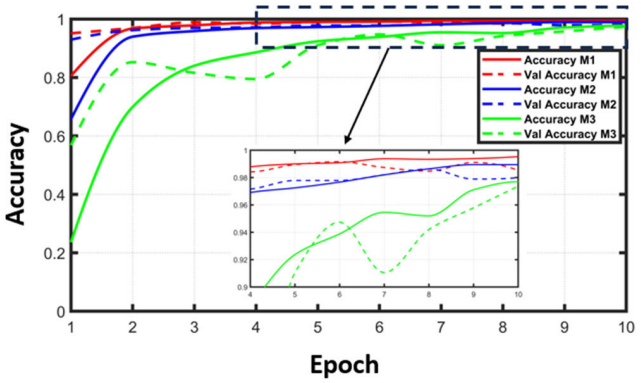

FIGURE 8. 15 classes model M1/ M2/ M3 performance.

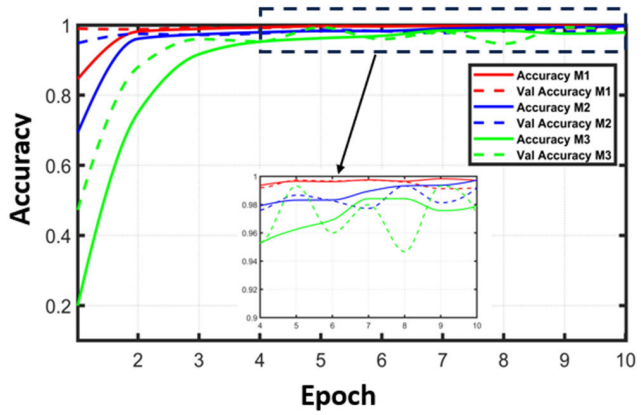

FIGURE 9. 17 classes model M1/ M2/ M3 performance.

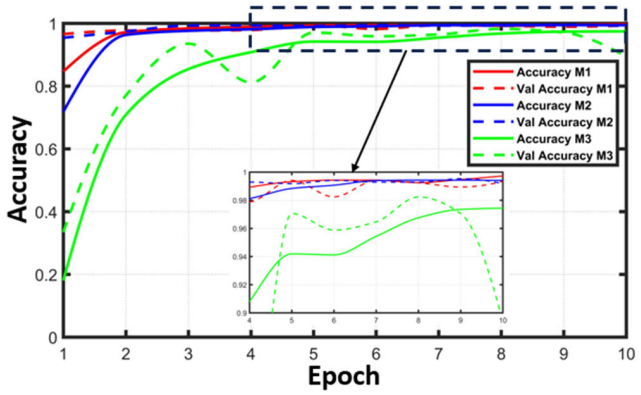

FIGURE 10. Classes model M1/ M2/ M3 performance.

indicating their capacity to adjust to shifting signal conditions. The results emphasize the delicate link between class count, model correctness, and complexity. As the number of classes increases, models become increasingly complicated to distinguish a larger collection of entities efficiently. These findings underline the necessity of carefully assessing the class distribution and its impact on model behaviour, particularly in scenarios combining diverse classes and demanding signal conditions.

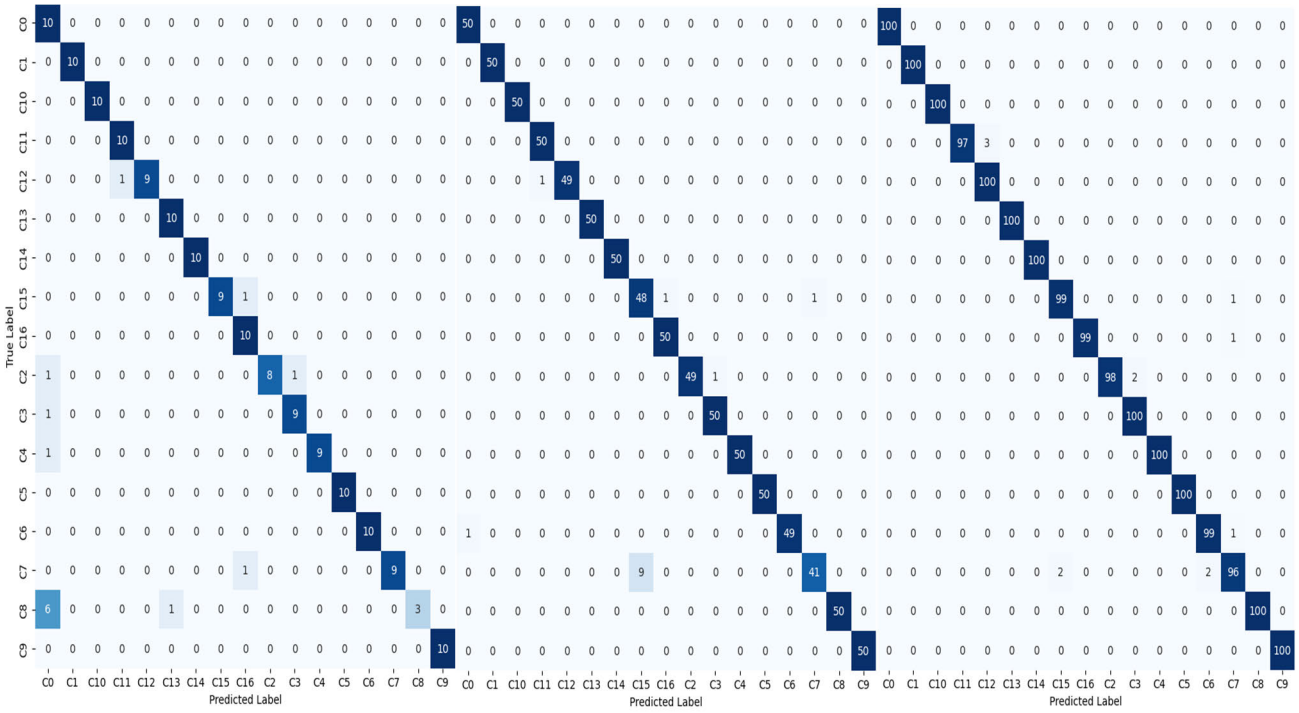

FIGURE 11. Classes model M1/M2/M3 confusion matrices.

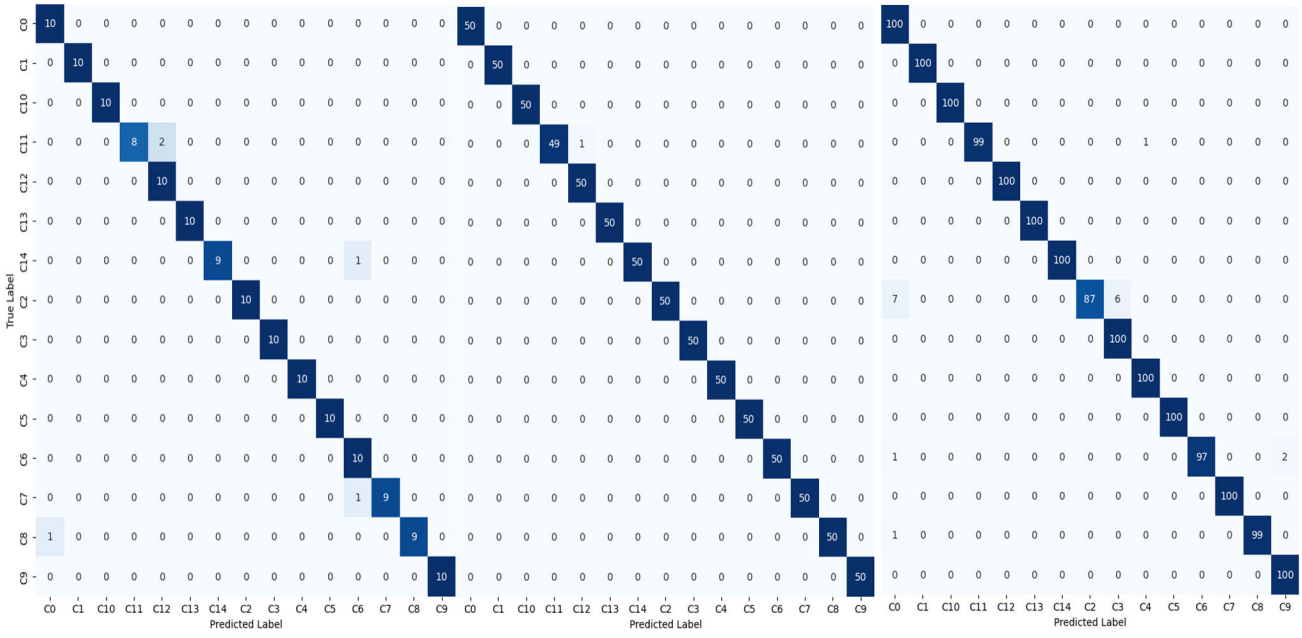

FIGURE 12. 17 classes model M1/M2/M3 confusion matrices.

1) NOISE: A COMPARATIVE ANALYSIS

Table 11 presents the accuracy percentages for different classes under three signal-to-noise ratio (SNR) conditions: 40dB, 30dB, and 20 dB to evaluate our models in different noise environments. Higher SNR generally leads to improved accuracy, while lower SNR levels decrease accuracy, making it more challenging for the models. Different numbers of classes exhibit varying levels of accuracy, indicating different performance for each class. These models demonstrate the ability to handle

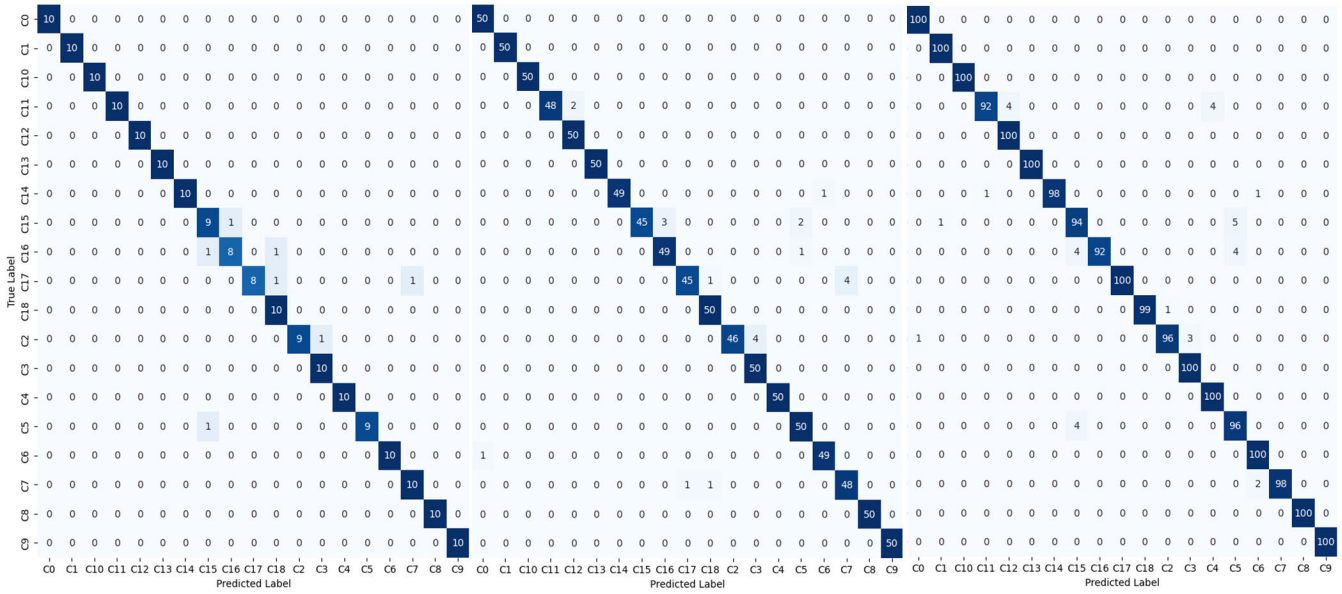

FIGURE 13. 19 classes model M1/M2/M3 confusion matrices.

TABLE 10. Performance evaluation of models with 15, 17, and 19 classes.

		Test Accuracy			with 30dB SNR		
M	% of Data	15 classes (%)	17 classes (%)	19 classes (%)	15 classes (%)	17 classes (%)	19 classes (%)
1	100	98.80	99.29	98.16	99.40	99.59	99.05
2	50	99.87	98.35	97.79	99.60	97.53	97.79
3	10	96.67	95.29	96.32	95.33	92.63	93.53

TABLE 11. Performance evaluation: noisy environments.

Classes	40dB SNR (%)	30dB SNR (%)	20dB SNR (%)
15	99.20	99.60	96.53
17	99.18	97.53	97.18
19	97.37	97.79	95.68

diverse noise environments, albeit with different degrees of success.

2) 60HZ VS. 50HZ: A COMPARATIVE ANALYSIS

To conclude our analysis of various environments, we will compare the global frequency environments of 50 Hz and 60 Hz. Table 12 compares 60 Hz, and 50 Hz class identification based on 50 samples, using 50% of the data, with the number of classes set at 15, 17, and 19. The findings indicate that the results are pretty similar, suggesting that the frequency values of 50 Hz and 60 Hz do not significantly impact the performance of the models.

V. IMPLICATIONS FOR PROTECTIVE RELAY

In this section, we will discuss the applicability of the proposed PQD identification technique in protection relay operations. Figure 14 shows the functional diagram of an automatic circuit recloser where the current and voltage data are sampled by the relay using a current transformer and voltage transformer through the switchgear interfacing module. The sampling rate of voltage and current may vary depending on the purpose of usage, e.g., measurement, monitoring protection, etc. To investigate the applicability of the proposed PQD identification model in protection relays, we studied the sampling rate of popular relays used in grid networks. The ABB REF615 relay, dedicated to protecting, measuring, controlling, and supervising overhead lines and cable feeders, has a sampling frequency of 32 samples per cycle [38]. Hence, it takes 1600 samples per second in a 50 Hz system and 1920 samples per second in a 60 Hz system. The analogue sampling frequency of Siemens SIPROTEC 5 overcurrent protection relay (7SJ82/7SJ85) is 16 kHz (sampling rate: 320 samplings per 50-Hz cycle) [39]. Upon correcting the magnitude, phase, and current-voltage transformer time constant, the sampling frequency is reduced to 8 kHz (160 samplings per 50-Hz cycle) [39]. Popular Australian-made automatic circuit reclosers use RC-10 and RC-15 relays in their control cubicle, the sampling rate of voltage and current of which is again reported to be 1600 samples/sec in a 50Hz system [40].

The sampling frequency of the simulations in this study was 10 kHz. To investigate the impact of sampling frequency on the accuracy of the CNN-based PQD detection model, simulations were done at higher sampling frequencies, e.g., 20, 50, and 100 kHz. The study demonstrated minimal improvement in fault detection accuracy at a higher sampling rate while the simulation time rose exponentially. A higher sampling rate also consumes more processing time in relays. Therefore, the overall sampling frequency used in this work (10 kHz) is suitable for application in conventional protection relays

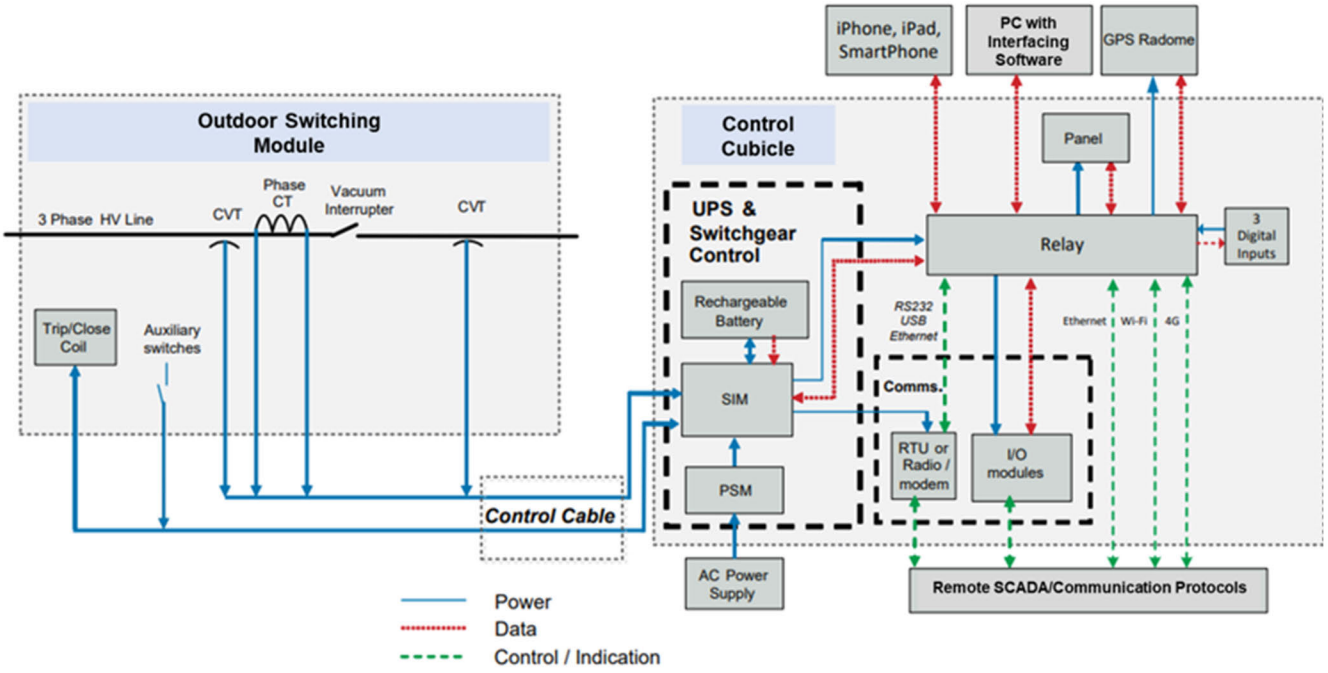

FIGURE 14. Functional structure of an automatic circuit recloser with control cubicle. Abbreviations in the figure: SIM = switchgear interfacing module, PSM = power supply module, RTU = remote terminal unit, CT = current transformer, CVT = capacitive voltage transformer [40].

VI. CONCLUSION AND FUTURE WORK

This study introduces the application of simple CNN models for detecting and classifying power quality disturbances, highlighting their adaptability and robustness. The novelty of this work lies in its focus on evaluating the performance of lightweight CNN architectures across diverse scenarios, including varying numbers of classes, SNRs, and frequencies, without relying on highly complex model configurations. By systematically testing multiple model configurations, the study demonstrates that even simple CNN models can achieve substantial accuracy levels in both normal and noisy environments, overcoming challenges typically associated with increased complexity, such as the inclusion of additional disturbance types. This work uniquely underscores the feasibility of employing lightweight CNNs for PQD classification tasks, offering a cost-effective and computationally efficient solution compared to more complex architectures. Furthermore, the adaptability of these models suggests their potential for deployment in real-world applications where robustness to noise and scalability to diverse disturbance types are critical. Future advancements could explore optimizing CNN architectures with more advanced hyperparameter tuning and integrating diverse, realistic datasets to further enhance their utility and reliability in practical power quality monitoring systems.

REFERENCES

[1] A. Mahlobo, O. Emmanuel Oni, and K. T. Akindeji, "Voltage fluctuation correction for renewable energy systems in distribution network," in *Proc. Int. Conf. Electr., Comput. Energy Technol. (ICECET)*, Nov. 2023, pp. 1–7, doi: 10.1109/ICECET58911.2023.10389256.

[2] P. W. Sauer, M. A. Pai, and J. H. Chow, *Power System Dynamics and Stability: With Synchrophasor Measurement and Power System Toolbox 2E*. Hoboken, NJ, USA: Wiley, 2017, doi: 10.1002/9781119355755.

[3] X. Liang, "Emerging power quality challenges due to integration of renewable energy sources," *IEEE Trans. Ind. Appl.*, vol. 53, no. 2, pp. 855–866, Mar. 2017, doi: 10.1109/TIA.2016.2626253.

[4] *IEEE Standard Requirements for Overhead, Pad Mounted, Dry Vault, and Submersible Automatic Circuit Reclosers and Fault Interrupters for AC Systems*, Standard IEEE Std C37.60-2003, 2003, pp. 1–71, doi: 10.1109/IEEESTD.2003.339580.

[5] *High-Voltage Switchgear and Control Gear—Part 111:, High-Voltage Switchgear and Controlgear—Part 111: Automatic Circuit Reclosers for Alternating Current Systems Up To and Including 38 KV*, Standard IEC 62271-111, 2019, doi: 10.1109/IEEESTD.2019.8641507.

[6] *High-voltage Switchgear and Controlgear—Part 200: High-Voltage Switchgear and Controlgear—Part 200: AC Metal-enclosed Switchgear and Controlgear for Rated Voltages Above 1 KV and Up To and Including 52 KV*, Standard IEC 62271-200, 2021.

[7] C. Cui, Y. Duan, H. Hu, L. Wang, and Q. Liu, "Detection and classification of multiple power quality disturbances using stockwell transform and deep learning," *IEEE Trans. Instrum. Meas.*, vol. 71, pp. 1–12, 2022, doi: 10.1109/TIM.2022.3214284.

[8] M. Shafiullah and M. A. Abido, "S-transform based FFNN approach for distribution grids fault detection and classification," *IEEE Access*, vol. 6, pp. 8080–8088, 2018, doi: 10.1109/ACCESS.2018.2809045.

[9] S. He, K. Li, and M. Zhang, "A real-time power quality disturbances classification using hybrid method based on S-transform and dynamics," *IEEE Trans. Instrum. Meas.*, vol. 62, no. 9, pp. 2465–2475, Sep. 2013, doi: 10.1109/TIM.2013.2258761.

[10] L. S. Pinto, M. V. Assunção, D. A. Ribeiro, D. D. Ferreira, B. N. Huallpa, L. R. M. Silva, and C. A. Duque, "Compression method of power quality disturbances based on independent component analysis and fast Fourier transform," *Electric Power Syst. Res.*, vol. 187, Oct. 2020, Art. no. 106428, doi: 10.1016/j.epsr.2020.106428.

[11] L. Sevgi, "Numerical Fourier transforms: DFT and FFT," *IEEE Antennas Propag. Mag.*, vol. 49, no. 3, pp. 238–243, Jun. 2007, doi: 10.1109/MAP.2007.4293982.

[12] H. Liu, H. Hu, H. Chen, L. Zhang, and Y. Xing, "Fast and flexible selective harmonic extraction methods based on the generalized discrete Fourier transform," *IEEE Trans. Power Electron.*, vol. 33, no. 4, pp. 3484–3496, Apr. 2018, doi: 10.1109/TPEL.2017.2703138.

[13] T. Srividya, A. M. Sankar, and T. Devaraju. (Jul. 2013). *Identifying, Classifying Of Power Quality Disturbances Using Short Time Fourier Transform and S-Transform*. Weekly Science. [Online]. Available: https://api.semanticscholar.org/CorpusID:14586055

[14] M. Sahani and P. K. Dash, "Automatic power quality events recognition based on Hilbert Huang transform and weighted bidirectional extreme learning machine," *IEEE Trans. Ind. Informat.*, vol. 14, no. 9, pp. 3849–3858, Sep. 2018, doi: 10.1109/TII.2018.2803042.

[15] M. Ijaz, M. Shafiullah, and M. A. Abido, "Classification of power quality disturbances using wavelet transform and optimized ANN," in *Proc. 18th Int. Conf. Intell. Syst. Appl. Power Syst. (ISAP)*, Sep. 2015, pp. 1–6, doi: 10.1109/ISAP.2015.7325522.

[16] J. Barros, R. I. Diego, and M. de Apraiz, "Applications of wavelet transform for analysis of harmonic distortion in power systems: A review," *IEEE Trans. Instrum. Meas.*, vol. 61, no. 10, pp. 2604–2611, Oct. 2012, doi: 10.1109/TIM.2012.2199194.

[17] C. Aneesh, S. Kumar, P. M. Hisham, and K. P. Soman, "Performance comparison of variational mode decomposition over empirical wavelet transform for the classification of power quality disturbances using support vector machine," *Proc. Comput. Sci.*, vol. 46, pp. 372–380, Jan. 2015, doi: 10.1016/j.procs.2015.02.033.

[18] K. Cai, W. Cao, L. Aarniovuori, H. Pang, Y. Lin, and G. Li, "Classification of power quality disturbances using wigner-ville distribution and deep convolutional neural networks," *IEEE Access*, vol. 7, pp. 119099–119109, 2019, doi: 10.1109/ACCESS.2019.2937193.

[19] P. D. Achlerkar, S. R. Samantaray, and M. S. Manikandan, "Variational mode decomposition and decision tree based detection and classification of power quality disturbances in grid-connected distributed generation system," *IEEE Trans. Smart Grid*, vol. 9, no. 4, pp. 3122–3132, Jul. 2018, doi: 10.1109/TSG.2016.2626469.

[20] S. Raza, H. Mokhlis, H. Arof, J. A. Laghari, and L. Wang, "Application of signal processing techniques for islanding detection of distributed generation in distribution network: A review," *Energy Convers. Manage.*, vol. 96, pp. 613–624, May 2015, doi: 10.1016/j.enconman.2015.03.029.

[21] D. Yadav, L. Sahoo, S. K. Mandal, G. Ravivarman, P. Vijayaraghavan, and B. Prasad, "Using long short-term memory units for time series forecasting," in *Proc. 2nd Int. Conf. Futuristic Technol. (INCOFT)*, Nov. 2023, pp. 1–6, doi: 10.1109/INCOFT60753.2023.10425756.

[22] L. Alzubaidi, J. Zhang, A. J. Humaidi, A. Al-Dujaili, Y. Duan, O. Al-Shamma, J. Santamaría, M. A. Fadhel, M. Al-Amidie, and L. Farhan, "Review of deep learning: Concepts, CNN architectures, challenges, applications, future directions," *J. Big Data*, vol. 8, no. 1, p. 53, Mar. 2021, doi: 10.1186/s40537-021-00444-8.

[23] H. Liao, J. V. Milanovic, M. Rodrigues, and A. Shenfield, "Voltage sag estimation in sparsely monitored power systems based on deep learning and system area mapping," *IEEE Trans. Power Del.*, vol. 33, no. 6, pp. 3162–3172, Dec. 2018, doi: 10.1109/TPWRD.2018.2865906.

[24] L. Chen, S. Chen, J. Xu, and C. Zhou, "Power quality disturbances identification based on deep neural network model of time-frequency feature fusion," *Electric Power Syst. Res.*, vol. 231, Jun. 2024, Art. no. 110283, doi: 10.1016/j.epsr.2024.110283.

[25] W. Zhaoqing, C. Yanzhao, C. Jianlei, and B. Weiyu, "Optimized decomposition and identification method for multiple power quality disturbances," *IET Gener., Transmiss. Distrib.*, vol. 18, no. 21, pp. 3501–3509, Nov. 2024, doi: 10.1049/gtd2.13200.

[26] M. Syamsudin, C.-I. Chen, S. S. Berutu, and Y.-C. Chen, "Efficient framework to manipulate data compression and classification of power quality disturbances for distributed power system," *Energies*, vol. 17, no. 6, p. 1396, Mar. 2024, doi: 10.3390/en17061396.

[27] I. S. Samanta, S. Panda, P. K. Rout, M. Bajaj, M. Piecha, V. Blazek, and L. Prokop, "A comprehensive review of deep-learning applications to power quality analysis," *Energies*, vol. 16, no. 11, p. 4406, May 2023, doi: 10.3390/en16114406.

[28] C. I. Garcia, F. Grasso, A. Luchetta, M. C. Piccirilli, L. Paolucci, and G. Talluri, "A comparison of power quality disturbance detection and classification methods using CNN, LSTM and CNN-LSTM," *Appl. Sci.*, vol. 10, no. 19, p. 6755, Sep. 2020, doi: 10.3390/app10196755.

[29] K. Cai, T. Hu, W. Cao, and G. Li, "Classifying power quality disturbances based on phase space reconstruction and a convolutional neural network," *Appl. Sci.*, vol. 9, no. 18, p. 3681, Sep. 2019, doi: 10.3390/app9183681.

[30] C.-M. Li, Z.-X. Li, N. Jia, Z.-L. Qi, and J.-H. Wu, "Classification of power-quality disturbances using deep belief network," in *Proc. Int. Conf. Wavelet Anal. Pattern Recognit. (ICWAPR)*, Jul. 2018, pp. 231–237, doi: 10.1109/ICWAPR.2018.8521311.

[31] H. Sindi, M. Nour, M. Rawa, Ş. Öztürk, and K. Polat, "A novel hybrid deep learning approach including combination of 1D power signals and 2D signal images for power quality disturbance classification," *Exp. Syst. Appl.*, vol. 174, Jul. 2021, Art. no. 114785, doi: 10.1016/j.eswa.2021.114785.

[32] E. Yiğit, U. Özkaya, Ş. Öztürk, D. Singh, and H. Gritli, "Automatic detection of power quality disturbance using convolutional neural network structure with gated recurrent unit," *Mobile Inf. Syst.*, vol. 2021, pp. 1–11, Jul. 2021, doi: 10.1155/2021/7917500.

[33] *Voltage Characteristics of Electricity Supplied by Public Distribution Systems*, Belgian Standard, Brussels, Belgium, 1994.

[34] *Testing and Measurement Techniques Power Quality Measurement Methods*, document IEC 61000-4-30, 2003.

[35] *IEEE Recommended Practice for Monitoring Electric Power Quality*, Standard IEEE 1159-2009 (Revision of IEEE Std 1159-1995), 2009, pp. 1–94, doi: 10.1109/IEEESTD.2009.5154067.

[36] N. Ari and M. Ustazhanov, "Matplotlib in Python," in *Proc. 11th Int. Conf. Electron., Comput. Comput. (ICECCO)*, Sep. 2014, pp. 1–6, doi: 10.1109/ICECCO.2014.6997585.

[37] Y. LeCun, Y. Bengio, and G. Hinton, "Deep learning," *Nature*, vol. 521, no. 7553, pp. 436–444, May 2015, doi: 10.1038/nature14539.

[38] ABB, *Feeder Protection and Control REF615 Application Manual*, document 1MRS756378, Rev. K, 2012.

[39] *SIPROTEC 5—Devices Protection, Automation and Monitoring*, Catalog SIPROTEC 5.01, 4th ed., Siemens, Munich, Germany, 2020.

[40] "Product guide 'OSM automatic circuit recloser 15kV 27kV 38kV models," NOJA Power Ltd, Brisbane, QLD, Australia, Tech. Rep. 250112-135731.

MOHAMMED F. AL-MASHDALI received the B.Sc. degree in electrical engineering from the King Fahd University of Petroleum and Minerals (KFUPM), Dhahran, Saudi Arabia, in 2024. He started his research career as an undergraduate student and completed a couple of research projects as a participant in the Summer Undergraduate Research Experience (SURE) Program, KFUPM. His research interests include power system stability, renewable energy integration, power electronics, and machine learning techniques.

ASIF ISLAM (Member, IEEE) received the B.Sc. and M.Sc. degrees in electrical engineering from Bangladesh University of Engineering and Technology (BUET), in 2009 and 2012, respectively, and the Ph.D. degree from The University of Queensland, Australia, in 2017. He is an Assistant Professor (Research) with the Interdisciplinary Research Center for Sustainable Energy Systems (IRC-SES), King Fahd University of Petroleum and Minerals (KFUPM). Previously, he was a T&E Ops. Quality Manager with Boeing-Australia, from 2021 to 2023; a Test Engineer of power system protection with the HV Test Laboratory, NOJA Power, from 2018 to 2021; an Research and Development Engineer with NOJA Power, from 2013 to 2017; an Assistant Engineer with Power Grid Company of Bangladesh (PGCB) Ltd., from 2012 to 2013; and a Testing Engineer with Energypac Engineering Ltd., from 2009 to 2012. His research project is focused on developing a new type of simple air-based load-current switching device for MV networks. His research interests include power system protection, high voltage engineering, transformer and switchgear, and quality management systems. He is a member of Engineers Australia.

ABDULBASIT HASSAN (Student Member, IEEE) received the B.Eng. degree in mechatronics from Bayero University, Kano, Nigeria, in 2018. He is currently pursuing the M.Sc. degree in systems and control engineering with the Control and Instrumentation Engineering Department, King Fahd University of Petroleum and Minerals, Dhahran, Saudi Arabia. He is also a Graduate Assistant with the Air Force Institute of Technology (AFIT), Nigeria. His areas of interests include automation and robotics, control and optimization of energy systems, and artificial intelligence.

MD SHAFIULLAH (Senior Member, IEEE) received the B.Sc. and M.Sc. degrees in electrical and electronic engineering (EEE) from Bangladesh University of Engineering and Technology (BUET), Bangladesh, in 2009 and 2013, respectively, and the Ph.D. degree in electrical power and energy systems from the King Fahd University of Petroleum and Minerals (KFUPM), Saudi Arabia, in 2018. He was a Faculty Member of the Department of Electrical and Electronic Engineering, International Islamic University of Chittagong (IIUC), Bangladesh, from 2009 to 2013. He is currently an Assistant Professor with the Control and Instrumentation Department and a Research Affiliate with the Interdisciplinary Research Center for Sustainable Energy Systems (IRC-SES), KFUPM. His research interests include grid fault diagnosis, grid integration of renewable energy resources, power quality analysis, power system control and stability, evolutionary algorithms, and machine learning techniques.

MUJAHED AL-DHAIFALLAH (Member, IEEE) received the B.Sc. and M.Sc. degrees in systems engineering from the King Fahd University of Petroleum and Minerals (KFUPM), Dhahran, Saudi Arabia, and the Ph.D. degree in electrical and computer engineering from the University of Calgary, Calgary, AB, Canada. Since 2020, he has been an Associate Professor in systems engineering with KFUPM. He is also a Research Affiliate with the Interdisciplinary Research Center for Sustainable Energy Systems (IRC-SES), KFUPM. His current research interests include nonlinear systems identification, control systems, optimization, artificial intelligence, and renewable energy.

KHALID AL FUWAIL (Member, IEEE) received the B.Sc. degree in control and instrumentation engineering with a concentration in robotics and autonomous systems from the King Fahd University of Petroleum and Minerals (KFUPM), Dhahran, Saudi Arabia, in 2024. As an undergraduate student, he actively participated in many research applications and completed multiple projects, including the Renewable Energy Technical Incubator (RETI) Program and Undergraduate Student Research Grant Undergraduate Research Experience (URO) Program at KFUPM. His research interests include robotics, autonomous systems, control systems, renewable energy, and artificial intelligence applications.